Relationship between the Growth of Carbon Nanofilaments and Metal Dusting Corrosion

Z. Zeng* and K. Natesan

Energy Technology Division, Argonne National Laboratory, Argonne, Illinois 60439

Received April 4, 2005. Revised Manuscript Received May 4, 2005

Raman scattering, X-ray diffraction, scanning electron microscopy, and transmission electron microscopy were used to study the mechanism of the catalytic crystallization of carbon and metal dusting corrosion. A mechanism is proposed for both metal dusting and the growth of carbon fibers. Carbon cannot crystallize well by deposition from carburizing gases at low temperature without catalytic activation because of its strong C−C bonds and high melting temperature. To form good crystalline carbon, the carbon atoms must dissolve, diffuse through metal particles, and crystallize on an appropriate facet that can act as a template to help the epitaxial growth of carbon crystals. In this process, metal particles are liberated from the pure metal and alloys. This liberation leads to the metal dusting phenomenon. The catalytic growth of carbon filaments is due to the transportation of carbon from one facet of a metal or carbide particle that favors carbon deposition to another facet that favors carbon precipitation. The free energy of poor crystalline carbon is higher than that of good crystalline carbon. The decrease in free energy from highly disordered carbon to well-ordered carbon is the driving force for metal dusting and for growth of carbon filaments through metal particles.

Introduction

Recently, the growth of carbon nanotubes has attracted much attention because these nanotubes have many potential applications in electronic devices and as a hydrogen storage medium.[1−5] Meanwhile, metal dusting corrosion has been a long-standing problem in the petrochemical, syngas, and other industries.[6−17] This corrosion, which occurs in a strong carburizing gas at high temperature, is accompanied by the formation of carbon filaments (including carbon nanotubes and nanofibers), fine metal carbide, and/or pure metal. Although both nanofilament growth and metal dusting research involve the growth of carbon nanotubes, the two phenomena are usually studied separately. In this paper, we try to achieve a complete picture by examining the two phenomena as an entirety, so we can improve our understanding of the mechanism of both metal dusting and carbon filament growth.

Nanoparticles of nickel and iron are used as catalysts to grow carbon filaments. How these metal particles help the growth of carbon nanotubes or nanofibers is unclear. In 1972, Baker[18] proposed a metal-particle-assisted mechanism for the growth of carbon filaments that involves diffusion of carbon through the metal particle from the hotter leading face, on which exothermic decomposition of the hydrocarbon occurs, to the cooler trailing face, on which carbon is deposited from solution. The temperature gradient was reported as the driving force for the diffusion of carbon through the metal particle and for the growth of carbon filaments. But this mechanism fails to explain the growth of carbon fibers by pyrolysis of methane,[19] which is an endothermic decomposition reaction. Gorbunov et al.[20] proposed a solid−liquid−solid mechanism. They argued that the melting temperature of nanoparticles of nickel, cobalt, and iron may decrease from their regular melting temperature (>1300 °C), and the liquid metal phases will aid the growth of carbon nanotubes. However, the growth of carbon filaments was reported at a temperature as low as 352 °C,[21] and it is difficult to explain how nickel can melt at such a low temperature. Rostrup-

* To whom correspondence should be addressed. E-mail: zeng@anl.gov.

(1) Iijima, S. *Nature* **1991**, *354*, 56.
(2) Liu, C.; Fan, Y. Y.; Liu, M.; Cong, H. T.; Cheng, H. M.; Dresselhaus, M. S. *Science* **1999**, *286*, 1127.
(3) Deheer, W. A.; Chatelain, A.; Ugarte, D. *Science* **2001**, *270*, 1179.
(4) Fan, S. H.; Chapline, M. G.; Tombler, T. W.; Cassell, A. M.; Dai, H. J. *Science* **2003**, *283*, 512.
(5) Kong, J.; Franklin, N. R.; Zhou, C.; Chapline, M. G.; Peng, S.; Cho, K.; Dai, H. *Science* **2003**, *287*, 622.
(6) Camp, E. Q.; Phillips, C.; Gross, L. *Corrosion* **1945**, *1*, 149. Camp, E. Q.; Phillips, C.; Gross, L. *Corrosion* **1959**, *15*, 627t.
(7) Lefrancois, P. A.; Hoyt, W. B. *Corrosion* **1963**, *19*, 360t.
(8) Hochman, R. F. In *Proceedings of the 4th International Congress on Metallic Corrosion*; Hamner, N. E., Ed.; National Association of Corrosion Engineers: Houston, TX, 1972; pp 258−263.
(9) Schueler, R. C. *Hydrocarbon Process.* **1972**, *51*, 73.
(10) Hochman, R. F. In *Proceedings of the Symposium on Properties of High-Temperature Alloys with Emphasis on Environmental Effects*; Foroulis, Z. A., Pettit, F. S., Eds.; The Electrochemical Society: Princeton, NJ, 1977; pp 715−732.
(11) Grabke, H. J.; Krajak, R.; Nava Paz, J. C. *Corros. Sci.* **1993**, *35*, 1141.
(12) Grabke, H. J.; Krajak, R.; Muller-Lorenz, E. M. *Werkst. Korros.* **1993**, *44*, 89.
(13) Pippel, E.; Woltersdorf, J. H.; Grabke, J.; Strauss, S. *Steel Res.* **1995**, *66*, 217.
(14) Grabke, H. J. *Mater. Corros.* **1998**, *49*, 303.
(15) Maier M.; Norton, J. F. *Mater. Corros.* **1999**, *50*, 640.
(16) Zeng, Z.; Natesan, K.; Maroni, V. A. *Oxid. Met.* **2002**, *58*, 147.
(17) Zeng, Z.; Natesan, K. *Chem. Mater.* **2003**, *15*, 872.
(18) Baker, R. T. K.; Barber, M. A.; Feates, F. S.; Waite, R. J. *J. Catal.* **1972**, *26*, 51.
(19) Rostrup-Neilson, J. R. *Steam Reforming Catalysts*; Danish Technical Press: Copenhagen, 1975.
(20) Gorbunov, A.; Jost, O.; Pompe, W.; Graff, A. *Carbon* **2002**, *40*, 113.
(21) MaCarty, J. G.; Hou, P. Y.; Sheridan, D.; Wise, H. In *Coke Formation on Metal Surfaces*; Albright, L. F.; Baker, R. T. K., Eds.; ACS Symposium Series 202; American Chemical Society: Washington, DC, 1982; p 253.

10.1021/cm050712u CCC: $30.25
Published on Web 06/07/2005

Table 1. Composition (in wt %) of Specimens Used in the Study

specimen	Fe	Ni	Cr	C	Mn	Si	Mo	Al	others
253MA	65.4	10.9	20.9	0.09	0.6	1.6	0.3		N 0.19, Ce0.04
MA956	74.4		20.0					4.5	Ti 0.5, Y_2O_3 0.6
45TM	26.7	46.4	27.4	0.08	0.4	2.7			RE 0.07
Fe	99.9								
Ni	99.9								

Nielsen[22] proposed a concentration-driven mechanism for the nickel-assisted growth of carbon whiskers. This mechanism is attractive, but it is not clear why carbon must diffuse through the metal particle and precipitate on the other side instead of just precipitating on the surface where it is deposited.[22] Other mechanisms cannot totally explain the catalytic growth of carbon filaments either.[23]

The mechanism of metal dusting is also not clear. Hochman[10] proposed a mechanism for the metal dusting of iron that was studied extensively by Grabke et al.[11,13,14] The steps involved in this mechanism are the following: (a) carbon transfers from the gas atmosphere to metal surface and dissolves into the metal; (b) Fe_3C forms as carbon diffuses into the iron, and the metal becomes supersaturated; (c) metastable Fe_3C decomposes to Fe and graphite by the reaction $Fe_3C = 3Fe + C$. According to this mechanism, the final products are graphite and iron. However, instead of iron, Fe_3C is usually observed in the final product of metal dusting. It is not clear what drives both the formation and decomposition of Fe_3C under the same conditions of temperature, pressure, and gas composition. Therefore, the mechanism of metal dusting, which is always accompanied by the growth of carbon filaments, must be investigated further. The question is whether a close relationship exists between the two phenomena. Recent studies of the growth of carbon nanotubes have provided substantial information about the growth mechanism, and the development of new nanotechnology has stimulated the effort to revisit the mechanism of metal dusting corrosion.

Experimental Section

Alloys 253MA, MA956, and 45TM, and iron and nickel were selected for metal dusting experiments; their compositions are shown in Table 1. All specimens were polished with 400 grit SiC paper. Tests were conducted in a horizontal furnace, where the specimens were hung in an alumina boat for exposure to a flowing carburizing atmosphere at 1100 °F (593 °C). Two gas mixtures were used for the experiments. Gas 1 consisted of 72.4:8.1:17.2:2.3 $H_2/CO_2/CO/H_2O$, whereas Gas 2, a simulation of a reformer outlet gas, consisted of 53.4:5.7:18.4:22.5 $H_2/CO_2/CO/H_2O$. System pressure in the tests varied from 1 to 41 atm.

After each exposure period, the specimen weight change was determined after removal of adhering coke in an ultrasonic acetone bath. The microstructure of each sample was examined with a JSM-6400 scanning electron microscope. To study metallographic cross sections, the samples were electrolytically etched with 10% acetic acid at 10 V for 30 s. Electron diffraction patterns were collected by a Philips CM 30 transmission electron microscope.

Raman spectra were excited with 60 mW of 476-nm radiation from a Kr-ion laser. The incident beam impinged on the sample at an angle ~45° from the normal. Scattered radiation was collected along the surface normal with an f/1.4 lens and was analyzed with a triple Jobin−Yvon grating spectrometer and a CCD detector. All of our spectra were acquired for 300 s at room temperature.

Results and Discussion

Pure iron and nickel specimens were severely attacked by carbon. The weight loss rate of iron was greater than that of nickel. After exposure in the carburizing gas, iron and nickel specimens were embedded in fine black powder, conventionally called "coke". The Fe-base Alloys 253MA and MA956 were not attacked by metal dusting after 100 h of exposure. However, in carburizing gas 1 at 593 °C, metal dusting pits were observed on both alloys after 800 h of exposure. The corrosion rate of Ni-base Alloy 45TM was much lower than that of Fe-base alloys. However, ~936-μm metal dusting pits were observed after 3700 h of exposure in the carburizing gas (Figure 1). Figure 2, obtained by scanning electron

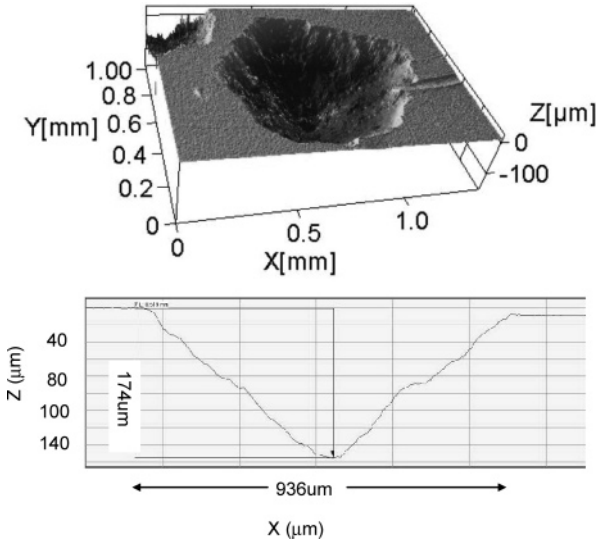

Figure 1. Alloy 45TM after 3700-h exposure in Gas 2, 53:5:18:23 $H_2/CO_2/CO/H_2O$, at 593 °C. Three-dimensional profile map shows metal dusting pit with depth of 174 μm and diameter of 936 μm.

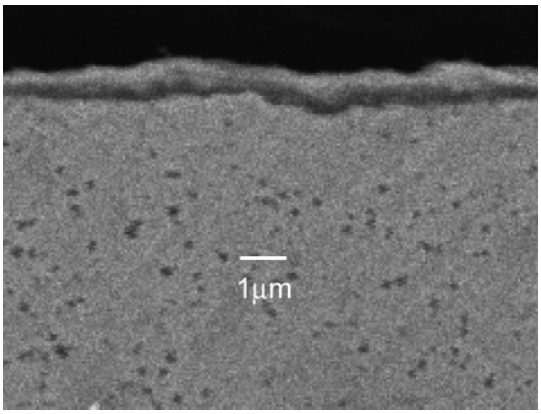

Figure 2. SEM microphotograph of cross section of Alloy 45TM after 3700-h exposure in Gas 2 (53:6:18:23 $H_2/CO_2/CO/H_2O$) at 593 °C, showing ~1-μm-thick oxide scale.

(22) Rostrup-Nielsen, J.; Trimm, D. L. *J. Catal.* **1977**, *48*, 155.
(23) Yang R. T.; Chen, J. P. *J. Catal.* **1989**, *115*, 52.

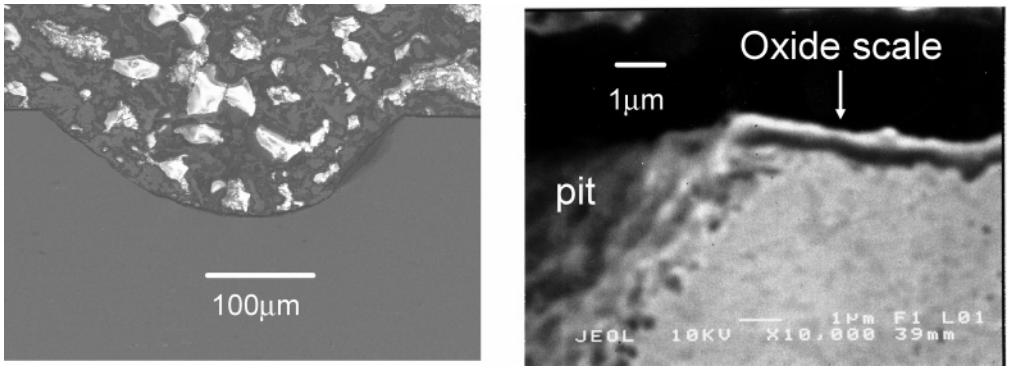

Figure 3. SEM microphotograph of cross section of Alloy 45TM after 3700-h exposure in Gas 2 (53:6:18:23 $H_2/CO_2/CO/H_2O$) at 593 °C. Left: metal dusting pit. Right: oxide scale broken in vicinity of pit.

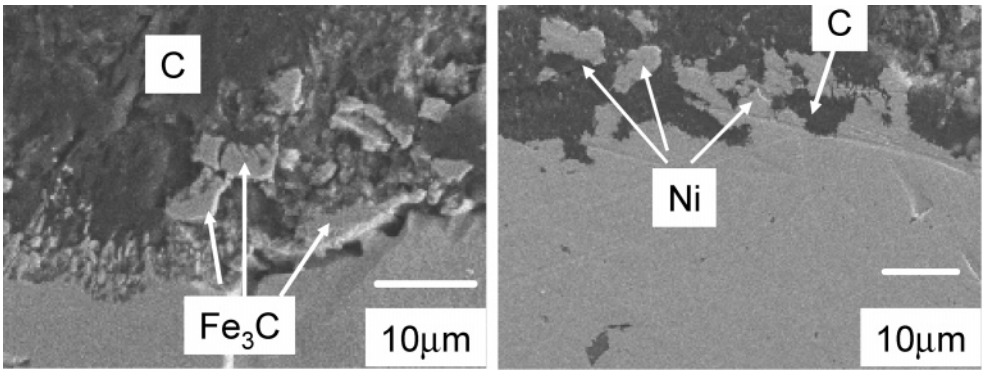

Figure 4. SEM microphotograph of cross section of (left) iron and (right) nickel specimens after metal dusting test.

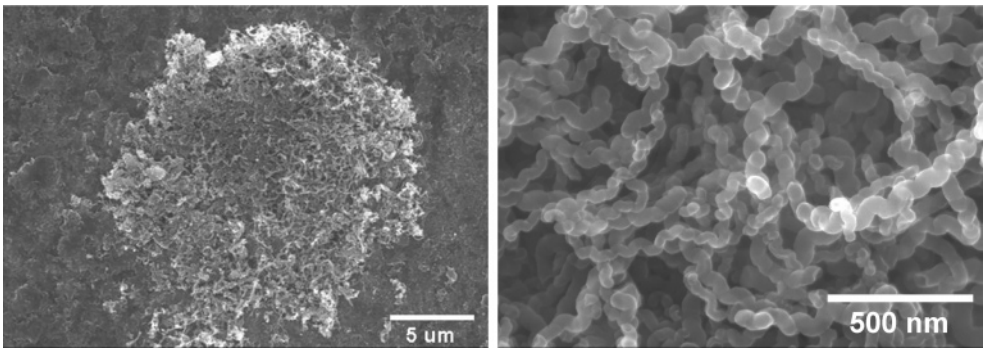

Figure 5. Left: Carbon filaments in a metal dusting pit on Alloy 45TM. Right: Higher magnification of pit region.

microscopy (SEM), shows an ~1-μm-thick oxide scale in the regions of Alloy 45TM that contained no pits. Oxide scales were also observed on Alloys 253MA and MA956, but not on pure iron and nickel.

Both Cr_2O_3 and spinel $FeCr_2O_4$ were observed by Raman spectroscopy. The most intense Raman band from Cr_2O_3 is the peak at 551 cm^{-1}. The band at 683 cm^{-1} corresponds to spinel.[24,25] Although these oxide scales protect alloys from metal dusting corrosion, they were broken at the pit area, as shown in Figure 3. Carburizing gases directly contacted metallic alloys and led to continuation of metal dusting corrosion at the pit area.

The metallographic photographs for iron and nickel (see Figure 4) show that iron carbide and nickel are separated into small particles in the surface regions of the specimens during the metal dusting process. Our X-ray diffraction (XRD) results and magnetization measurements indicate that the major phases in the metal dusting product of iron are carbon and Fe_3C.[16] Toh et al.[26] used transmission electron microscopy (TEM) to analyze these particles, and identified them as Fe_3C. The major phases in the metal dusting product of nickel specimens are carbon and nanosize nickel particles. Ni_3C is not stable under our experimental condition and none was observed.

In general, most of the coke consisted of carbon filaments that are ~20−1000 nm in diameter. Figure 5 shows that carbon filaments grew out from a metal dusting pit. The diameter of the carbon filaments that grew on the surface of the iron was similar to that of the carbon filament that grew on the surface of nickel. Carbon filaments that formed under high system pressure were usually larger in diameter than those formed at 1 atm. A nanosize iron carbide or nickel

(24) Farrow, R. L.; Benner, R. E.; Nagelberg, A. S.; Mattern, P. L. *Thin Solid Films* **1980**, *73*, 353.
(25) Thierry, D.; Persson, D.; Leygraf, C.; Delichere, D.; Joiret, S.; Pallotta, C.; Hugot-Le Goff, A. *J. Electrochem. Soc.* **1988**, *135*, 305.
(26) Toh, C. H.; Munroe, P. R.; Young, D. J. *Oxid. Met.* **2002**, *58*, 1.

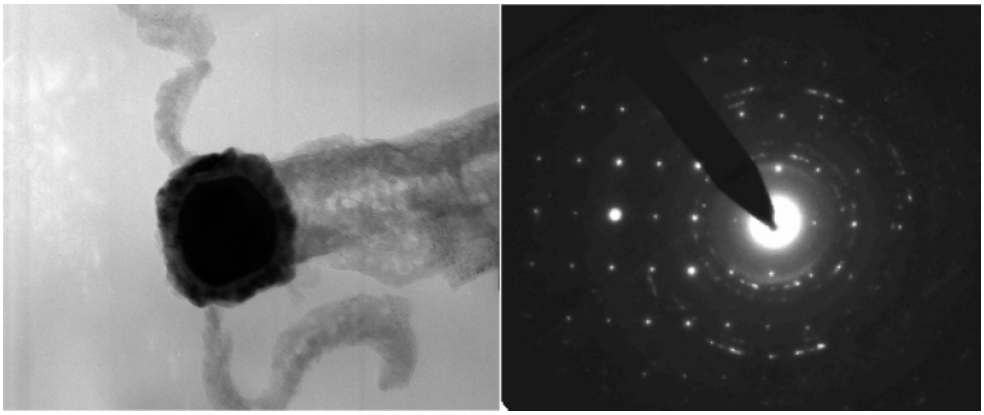

Figure 6. Left: Carbon filament with particle at tip. Carbon filament was product of metal dusting in iron after 100-h exposure in Gas 1 at 593 °C. Right: Selected area diffraction pattern from particle at tip of carbon filament, indexed with [011] zone axis of Fe_3C.

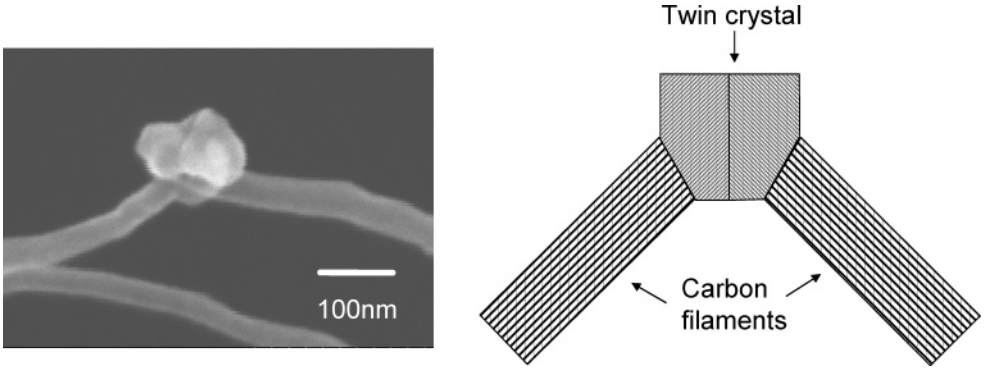

Figure 7. Left: SEM microphotograph of two carbon filaments that grew from a particle. Right: Particle may be twin crystal with differing orientations, which led to growth of two carbon filaments.

particle was usually observed at the tip of the carbon filaments. Figure 6 shows a TEM image of a particle at the tip of the carbon filament that grew from an iron specimen exposed in Gas 1. The selected area diffraction pattern from the particle can be indexed with the [011] zone axis of an orthorhombic phase with lattice parameters $a = 5.07$, $b = 6.73$, and $c = 4.52$. This phase should be Fe_3C. We did not observe any pure iron particles in coke by TEM, a result that is consistent with the finding of Toh et al.[26]

Both Fe3C and nickel particles acted as catalysts for the growth of carbon filaments. Carbon was absorbed from the top of the particles, and filaments grew in one direction from the bottom of the particles. However, in a few cases, particles were also observed in the middle of carbon filaments, which may indicate that filaments can grow in two directions. Figure 7 is an example in which two carbon filaments grew from one metal carbide particle, probably a twin crystal with differing orientations. Figures 8 and 9 show a particle in the middle of a carbon filament. Sea-urchin-like and weblike carbon nanotubes have also been reported.[27,28] It is difficult to explain the growth of this carbon filament by Baker's mechanism because temperature gradient will drive a carbon filament to grow in only one direction, not in two opposite directions. In general, the carbon filaments are of uniform diameter, but bamboo-like carbon filaments were observed. If the filament diameter is <50 nm, round hollow tubes were observed; if the diameter of the carbon filaments is >500 nm, carbon rods with round, square, and triangular cross sections are observed.

Table 2 shows that the crystallites of coke developed during metal dusting are much larger than crystallites of glassy carbon. The crystallites of coke observed in the present study are also considerably larger than crystallites reported for other carbonaceous materials made at a similar temperature.[29] The crystallites of coke on an iron surface are larger than those on a nickel surface.

The interlayer distances between the carbon planes are related to the degree of disorder.[29] In the disoriented graphite structure, the layers are not parallel, and the average interlayer planar distance increases with an increase in disorientation. Single-crystal graphite exhibits the smallest interlayer plane distance (3.354 Å), whereas the interlayer planar distance in coke is similar to that in well-crystallized graphite. For the carbon produced by conventional treatment of carbonaceous raw materials, a heat treatment temperature >2000 °C is required for thermal recrystallization to achieve this high degree of three-dimensional ordering.[29]

The Raman spectrum for well-crystallized graphite shows a sharp band at 1580 cm^{-1} (G band), which can be assigned to the E_{2g} C−C stretching mode.[30−32] The first-order phonon band at 1360 cm^{-1} (D band) is not observed for well-

(27) Gavillet, J.; Loiseau, A.; Ducastelle, F.; Thair, S.; Bernier, S.; Stephan, O.; Thibault, J.; Charlier, J.-C. *Carbon* **2002**, *40*, 1649.
(28) Yudasaka, M.; Yamada, R.; Sensui, N.; Wilkins, T.; Ichihashi, T.; Iijima, S. *J. Phys. Chem. B.* **1999**, *103*, 6224.
(29) Blayden, H. E.; Riley, H. L.; Taylor, A. *J. Am. Chem. Soc.* **1940**, *62*, 180.
(30) Tuinstra F.; Koenig, J. L. *J. Chem. Phys.* **1970**, *53*, 1126.
(31) Al-Jishi, R. *Phys. Rev. B* **1982**, *26*, 4514.
(32) Vidano R.; Fischbach, D. B. *J. Am. Ceram. Soc.* **1978**, *61*, 13.

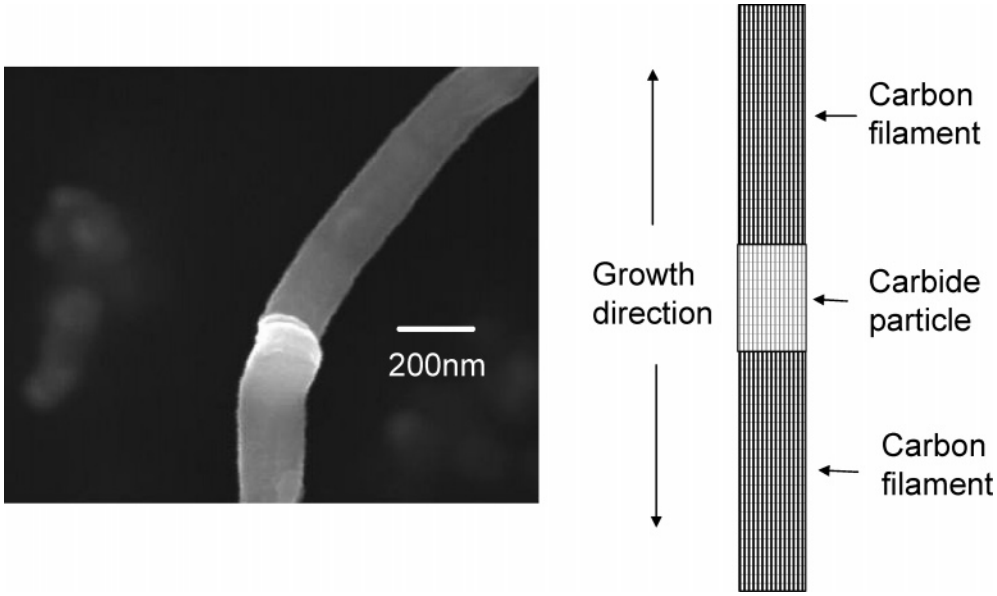

Figure 8. Left: SEM microphotograph of particle in middle of carbon filament. Right: schematic representation of carbon filaments growth in two directions.

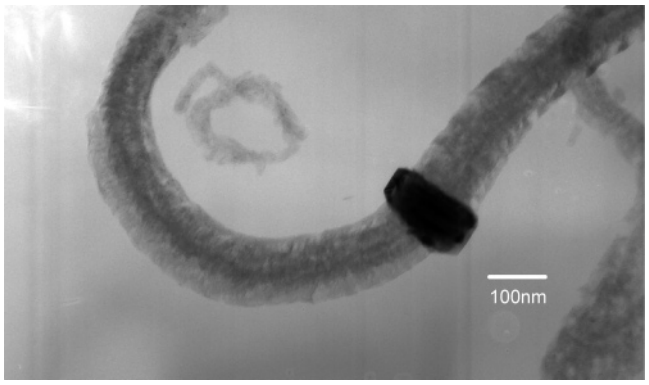

Figure 9. TEM image of particle in middle of carbon filament.

Table 2. Crystallite Dimensions and Interlayer Planar Distances in Graphite, Coke, and Glassy Carbon

carbon material	interlayer planar distance (Å)	Δ (Å)[a]	crystallite size (Å)		mean number of layers per particle
			c-axis	*a*-axis	
graphite	3.356	0.002	220	299	65.7
coke from Fe	3.365	0.011	110	127	32.8
coke from Ni	3.396	0.042	62.8	67.5	18.5
glassy carbon	3.736	0.382	12	15	3.4

[a] Δ is difference between interlayer planar distance of carbon in the material and that in single-crystal graphite (3.354 Å).

crystallized graphite because of the $k = 0$ selection rule.[30] However, disorder in the lattice can break down this selection rule, which is why the 1360 cm^{-1} band is observed in the Raman spectra of disordered carbon. Highly disordered carbon shows very broad Raman bands, and the intensity of the 1360 cm^{-1} band increases when carbon becomes more disordered. The shoulder at 1607 cm^{-1} in coke also depends on structural disorder and is, therefore, designated as the D′ band. The G band was not observed in glassy carbon because the D′ band is so strong that it obscures the G band. The bandwidths and the D/G intensity ratio are related to the crystallinity of the carbon dust.[30] The D band of coke is sharper than that of glassy carbon. Therefore, coke is better crystallized than glassy carbon.

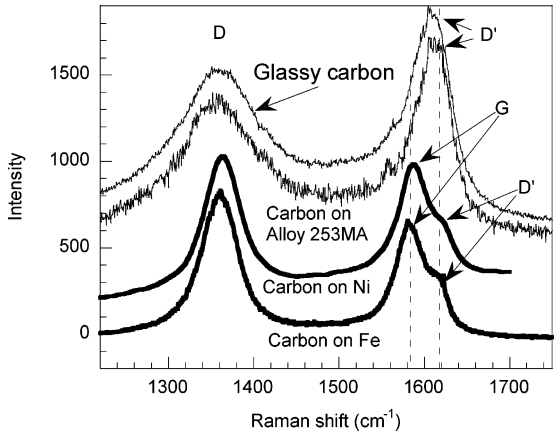

Figure 10. Raman spectra of highly disordered glassy carbon, and carbon deposited on surfaces of Alloy 253MA, iron, and nickel specimens.

Carbon that deposited on the surface of Alloy 253MA at 593 °C in 100 h shows bandwidths and shapes similar to those of glassy carbon (Figure 10). The oxide scale that formed on the surface of this alloy did not influence the crystallization of carbon. Therefore, the crystallinity of the carbon that deposited on the surface of Alloy 253MA is as poor as that in highly disordered glassy carbon. However, carbon on the surface of iron and nickel shows a band that is much sharper than that of glassy carbon, indicating that the crystallinity of this carbon is much better than that of glassy carbon and of the carbon on the surface of Alloy 253MA. Comparing the crystallinity of the carbon on Alloy 253MA, which was not attacked by metal dusting, with that of carbon on iron and nickel, which were attacked by metal dusting, we conclude that carbon crystallinity is poor when metal dusting was not initiated, whereas it is very good after metal dusting has progressed. Therefore, carbon crystallization is involved in the process of metal dusting.

Further evidence to support the idea that carbon crystallization is involved in metal dusting is the fact that carbon at the metal dusting pit area on Alloy MA956 and 45TM also shows a Raman band that is sharper than that of carbon deposited in the area without a pit (Figures 11 and 12).

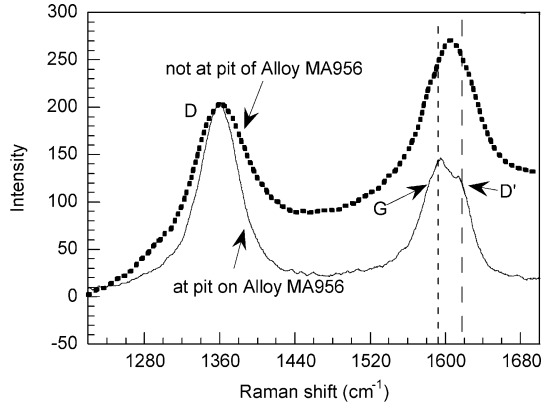

Figure 11. Raman spectra of carbon in pitted and nonpitted regions on surface of Alloy MA956, after exposure in metal dusting environment.

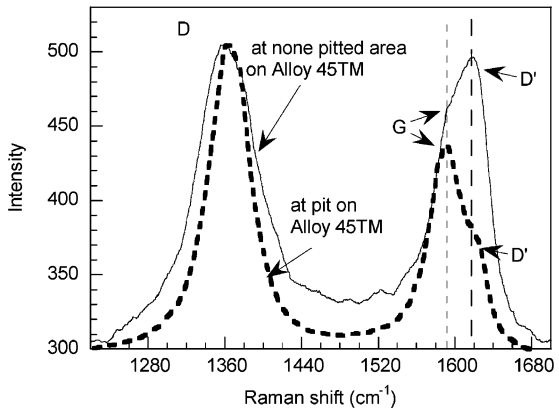

Figure 12. Raman spectra of carbon in pitted and nonpitted region on surface of Alloy 45TM, after exposure in metal dusting environment.

Graphite exhibits a layered structure with the space group $P6_3/mmc$. Carbon atoms within the layers bond strongly through sp^2 hybridization and form a two-dimensional honeycomb network. The layers are stacked in a hexagonal crystal structure and are bound together by van der Waals forces. Because the van der Waals force is weak, the C−C distance between layers is large (335.4 pm);[33] therefore, graphite crystals readily become disordered along the *c*-axis.[34]

At 593 °C, the recrystallization of carbon is difficult because the sp^2 C−C bond is strong and the melting temperature of carbon is high (4492 °C). Poorly crystallized carbon will form during the gas deposition process if no catalyst is present to aid the crystallization; carbon atoms would be held tightly and could not move to an optimum position whenever they were deposited from carbon-containing gases. Such poorly crystallized carbon was observed on the surface of Alloy 253MA, where deposited carbon is present on top of oxide scales that cannot aid the crystallization of carbon. However, when carbon is deposited on the surface of Ni or Fe_3C, it can dissolve into Ni or Fe_3C, and diffuse through the metal or carbide. Finally, carbon atoms find a favorite facet on which to precipitate out. When carbon atoms dissolve into metals or Fe_3C, their mobility is much greater than it is in graphite; therefore, carbon atoms can move to an optimum position and form good crystalline carbon. Metals and Fe_3C can aid the recrystallization of carbon. Because of the catalytic crystallization process, the crystallinity of coke produced by metal dusting is much better and the interlayer planar distance is smaller than it is in carbon made by other methods at a similar temperature. The interlayer binding energy of single-crystal graphite is ~3 kcal/mol,[35] and it decreases with an increase in interlayer planar distance.[36] It is estimated that, among the pyrolytic graphites, an enthalpy increment of 900 ± 200 J mol^{-1} increases interlayer planar distance by 2.1%.[37] The initial state of carbon that is deposited on the metal surface is very disordered. The free energy difference between this carbon and the well-crystallized graphite should be much larger than the difference between poly- and single-crystal graphite. The catalytic process leads to improved crystallization of carbon, with a reduction in the free energy from poorly crystallized carbon to that of well-crystallized carbon.

Carbon favors crystallization on a facet where the atomic distances on the facet match the lattice of graphite. For example, carbon precipitates on the [111] facet of Ni;[23] however, carbon deposition may favor another facet, e.g., [110] of Ni.[23] In the absence of a catalyst, the carbon deposition reaction ($CO + H_2 = C + H_2O$) proceeds with difficulty. Calculation shows that the reaction rate on the [110] facet of Ni is the fastest.[23] If the deposited carbon directly forms graphite on the [110] facet, poorly crystallized carbon will form, because the [110] facet does not match the graphite lattice. To form good crystalline carbon, carbon atoms must dissolve into and diffuse through the nickel, and finally precipitate on the [111] facet. The energy difference between poorly and well-crystallized carbon drives the transfer from one face of a metal to another. A similar process occurs with Fe_3C catalytic particles.[16]

When the above carbon crystallization process occurs in metals or alloys, carbon is transferred from the alloy surface and grows inward via the defects or grain boundary of the alloys. The accumulation of carbon in alloys causes the metal particles to disintegrate, as seen in Figure 4. When carbon continues to precipitate under the metal particle, a carbon filament is formed, as shown in Figure 5. The diagrams in Figures 13 and 14 schematically illustrate the entire sequence from metal dusting to carbon filament growth, and show that metal dusting is closely related to the growth of a carbon filament. Both carbon filament growth and metal dusting involve catalytic deposition of carbon and growth of graphite on the metal surface. Both processes have the same driving force, which is the free energy difference between poor and good crystalline carbon.

The metal dusting process leads the metals to separate into very small particles when carbon is continuously inserted into defects in the metals, as illustrated in Figure 4. When the metal particles at the tip of the carbon filament are very small, a carbon sheet follows the contour of the metal particle to fold into a tube, and the dangling bonds on the two edges of the sheet join (Figure 15). This process leads to a decrease in the system energy. If the particle is pear-shaped, multiwall

(33) Franklin, R. E. *Acta Crystallogr.* **1951**, *4*, 253.
(34) Krebs, H. *Fundamentals of Inorganic Crystal Chemistry*; McGraw-Hill: New York, 1968; p 150.
(35) Peacock, T. E. *J. Chem. Phys.* **1960**, *57*, 844.
(36) Lewis, D. C.; Frisch, M. A.; Margrave, J. L. *Carbon* **1965**, *2*, 431.
(37) Abrahamson, J. *Carbon* **1973**, *11*, 337.

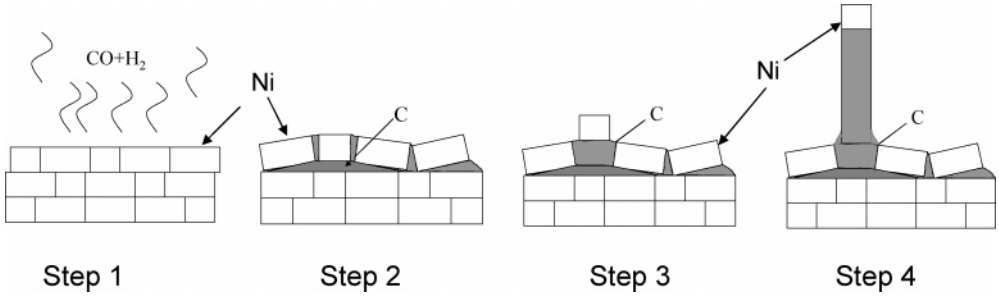

Figure 13. Process of metal dusting and carbon filament growth in Ni-base alloys. 1. Carbon deposits on surface of nickel. 2. Carbon dissolves and diffuses though Ni and precipitates at defects; accumulation of carbon at defects causes Ni particles to separate. 3. Gas penetrates into cracked areas and deposits carbon, and metal dusting corrosion proceeds further. 4. Carbon continues to precipitate under Ni particle and grows to carbon filament.

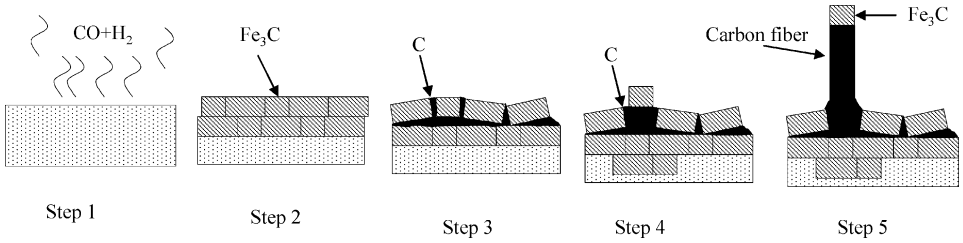

Figure 14. Process of metal dusting and carbon filament growth in Fe-base alloys. 1. Carbon deposits on iron surface. 2. Carbon dissolves in iron and forms Fe_3C, creating many defects as volume increases by ~10% when Fe_3C forms. 3. Carbon diffuses though Fe_3C and precipitates at defects; accumulation of carbon at defects causes Fe_3C particles to separate. 4. Gas penetrates into cracked areas and deposits carbon. More Fe_3C forms, and metal dusting corrosion proceeds further. 5. Carbon continues to precipitate under Fe_3C particle and grows to carbon filament.

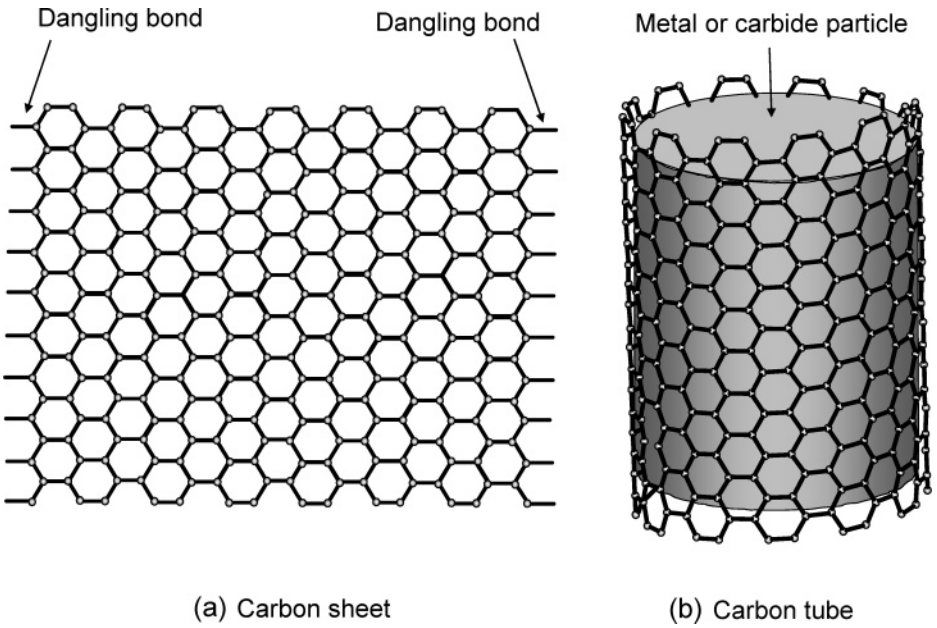

Figure 15. (a) Dangling bonds at edges of carbon sheet lead to high system energy. (b) When carbon sheet folds into a tube along a metal particle, system energy decreases.

nanotubes may grow by following the contour, as shown in Figure 16. Many researchers have observed a pear-shaped metal particle at the tip of a multiwall carbon nanotube.[22,38]

The driving force for the growth of both carbon nanorods and nanotubes is due to the decrease in free energy that occurs during carbon crystallization. This driving force always exists, and is independent of whether carbon deposition occurs by an exothermic or an endothermic reaction. If we assume that the driving force for carbon filament growth is temperature difference, it is difficult to understand why carbon filaments grow in both the exothermic and endothermic environments. However, if we assume that the driving force is the free energy difference between poor and good crystalline carbon, it is easy to understand this growth.

Our proposed mechanism of catalytic crystallization of carbon can explain the metal dusting process without involving the decomposition of Fe_3C. Nickel carbide does not form during the metal dusting process because it is unstable. Therefore, the mechanism for nickel has previously been considered different from that for iron.[39] However, if

(38) Sacco, A. J.; Geurts, F. W. A. H.; Jablonski, G. A.; Lee, S.; Gately, R. A. *J. Catal.* **1989**, *119*, 322.

(39) Grabke, H. J.; Krajak, R.; Muller-Lorenz, E. M.; Strauss, S. *Mater. Corros.* **1996**, *47*, 495.

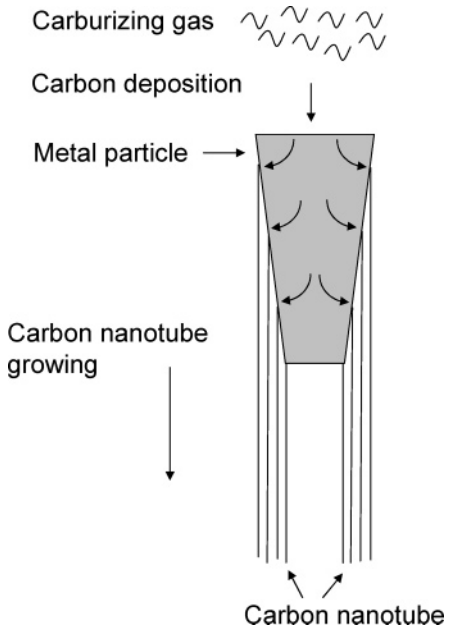

Figure 16. Multiwall nanotube growth following contour of pear-shaped metal particle.

the catalytic crystallization of carbon through iron carbide and nickel is similar, the dusting mechanism in both should be similar, although the process details may differ slightly. Metal dusting of both iron and nickel is caused by the catalytic crystallization of carbon and is driven by a similar force. Our study leads to a general mechanism for the metal dusting phenomenon.

Conclusions

The crystallinity of carbon that has experienced metal dusting is much better than that of carbon that has not experienced metal dusting. Both metal dusting and carbon filament growth are related to the catalytic crystallization of carbon. Carbon cannot crystallize well at low temperatures because of the strong C−C bond and its special layered structure. Carbon must dissolve and diffuse into a metal or carbide particle. This particle acts as a catalyst to aid the crystallization of carbon. In this catalytic crystallization process, metals are liberated into small particles and lead to metal dusting corrosion. The catalytic growth of carbon filaments is due to the transport of carbon from one facet of a metal or carbide particle that favors carbon deposition but not carbon precipitation to another facet that favors precipitation. The decrease of free energy from highly disordered carbon to well-crystallized carbon is the driving force for both catalytic growth of carbon filaments and metal dusting.

Acknowledgment. We thank V. A. Maroni and M. Grimsditch for their assistance in conducting the Raman analysis, and D. L. Rink for his assistance in conducting the metal dusting experiments. Special thanks to R. Koritala for her assistance with electron microscopy analysis. This work is supported by the U.S. Department of Energy, Office of Industrial Technologies, under Contract W-31-109-Eng-38. The SEM analysis was performed in the Electron Microscopy Center, Materials Science Division, Argonne National Laboratory, Argonne, IL.

CM050712U